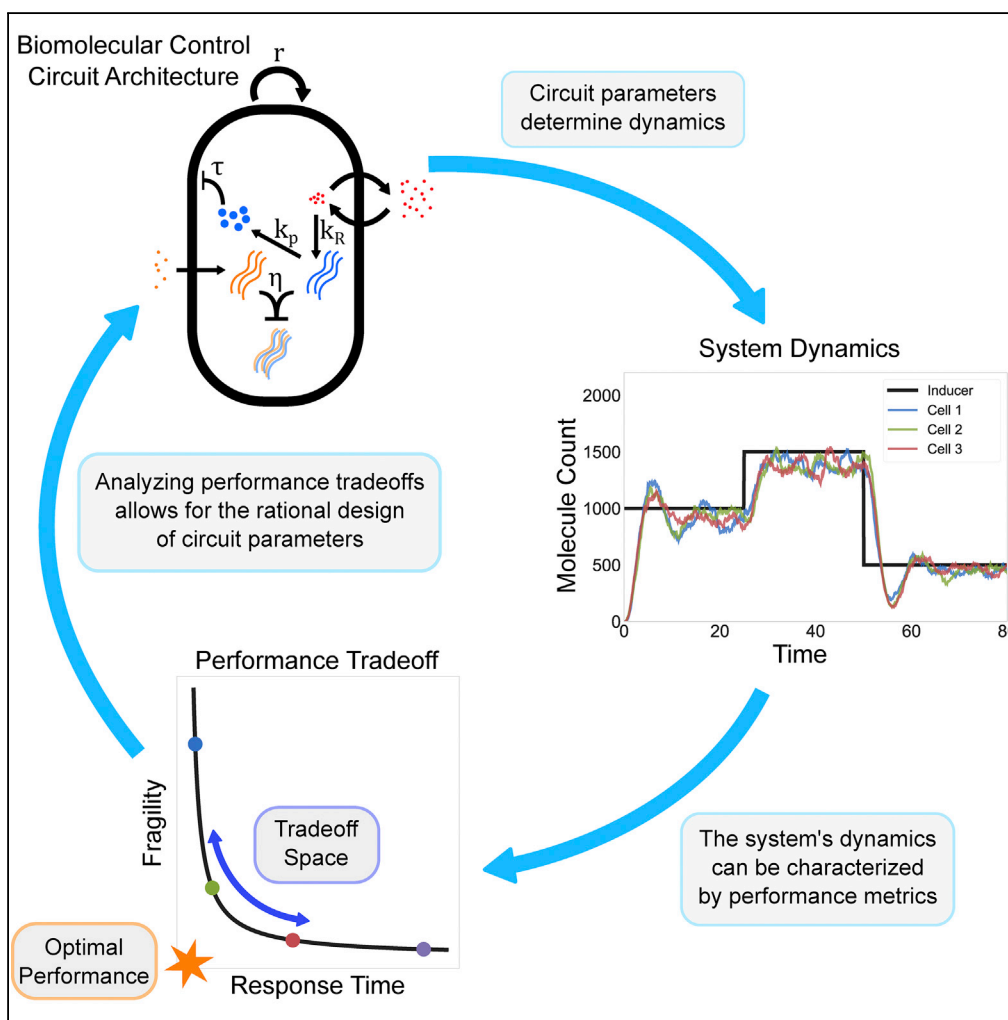**Article**

# Architectural Principles for Characterizing the Performance of Antithetic Integral Feedback Networks



Noah Olsman,
Fangzhou Xiao,
John C. Doyle

noah_olsman@hms.harvard.edu

**HIGHLIGHTS**

Control theory is used to characterize tradeoffs in a biomolecular control circuits

We show how low-level circuit parameters relate to high-level performance metrics

We provide a set of architectural principles for analyzing synthetic feedback circuits

## Article

# Architectural Principles for Characterizing the Performance of Antithetic Integral Feedback Networks

Noah Olsman,[1,2,4,*] Fangzhou Xiao,[3] and John C. Doyle[1,3]

## SUMMARY

As we begin to design increasingly complex synthetic biomolecular systems, it is essential to develop rational design methodologies that yield predictable circuit performance. Here we apply mathematical tools from the theory of control and dynamical systems to yield practical insights into the architecture and function of a particular class of biological feedback circuit. Specifically, we show that it is possible to analytically characterize both the operating regime and performance tradeoffs of an antithetic integral feedback circuit architecture. Furthermore, we demonstrate how these principles can be applied to inform the design process of a particular synthetic feedback circuit.

## INTRODUCTION

A present challenge in synthetic biology is to design circuits that not only perform a desired function, but also do so robustly. The difficulty in doing this arises in large part from the enormous amount of variability between both intracellular and extracellular environments (Elowitz and Leibler, 2000; Cardinale and Arkin, 2012; Paulsson, 2004; Swain et al., 2002; Lestas et al., 2010). Although it is becoming easier to quickly implement a given circuit architecture (Sun et al., 2013; Weber et al., 2011), ensuring that its performance is robust to parameter variations is still a time-consuming and challenging task (Potvin-Trottier et al., 2016). As synthetic circuits grow in size and complexity, it will be essential to develop a rational design methodology that allows biological engineers to easily identify the important design constraints for a given circuit and determine whether or not their desired behavior is feasible (Del Vecchio and Murray, 2015). We can draw inspiration from the study of natural biological circuits, where cells are frequently confronted with a large amount of variability, yet exhibit robust behavior at the system level (Goentoro and Kirschner, 2009; El-Samad et al., 2005; Cohen-Saidon et al., 2009; Barkai and Leibler, 1997; Yi et al., 2000; Chandra et al., 2011; Paszek et al., 2010).

In the design of electrical and mechanical systems this problem is often solved with the implementation of feedback control (Aström and Murray, 2008; Doyle et al., 2013), where the dynamics of a process are adjusted based on measurements of the system's state with the aim of achieving some performance goals. For example, in a commercial cruise control system an engineer may want the car to be able to rapidly track whatever reference speed the user desires by measuring the car's current velocity, while accelerating at a safe rate and not being too sensitive to small disturbances (e.g., road conditions). Similarly, a biological engineer may want the output concentration of a molecular species in a circuit to track an input signal (e.g., an inducer) with dynamics that are robust to parametric variability in reaction rates and the inherent noisiness of chemical kinetics (Hsiao et al., 2014).

Our primary focus here is a circuit architecture proposed by Briat et al. (2016), know as an antithetic integral feedback, that uses an irreversible binding mechanism to implement feedback control in a biomolecular circuit. This circuit immediately had a broad impact on the study of biological feedback systems, as strong binding is both abundant in natural biological contexts (Kampranis et al., 1999; Hamilton and Baulcombe, 1999; Zhou and Gottesman, 1998) and appears to be feasible to implement in synthetic networks (Qian et al., 2018; Qian and Del Vecchio, 2018; Franco et al., 2014; Nevozhay et al., 2009; Lillacci et al., 2018). For example, antithetic integral feedback can be implemented using sense-antisense mRNA pairs (Agrawal et al., 2018), sigma-antisigma factor pairs (Lillacci et al., 2017), or scaffold-antiscaffold pairs (Hsiao et al., 2014).

The purpose of this circuit is to control a process, a simple version of which is composed of the molecular species $X_1$ and $X_2$ with two control species $Z_1$ and $Z_2$ (Figure 1A). The goal is to set an external reference $\mu$ and have the concentration of the output species $X_2$ robustly track it (Figure 1B).

[1]Department of Control and Dynamical Systems, California Institute of Technology, 1200 E. California Boulevard, Pasadena, CA 91125, USA

[2]Department of Systems Biology, Harvard Medical School, 200 Longwood Avenue, Boston, MA 02215, USA

[3]Division of Biology and Biological Engineering, California Institute of Technology, 1200 E. California Boulevard, Pasadena, CA 91125, USA

[4]Lead Contact

*Correspondence: noah_olsman@hms.harvard.edu

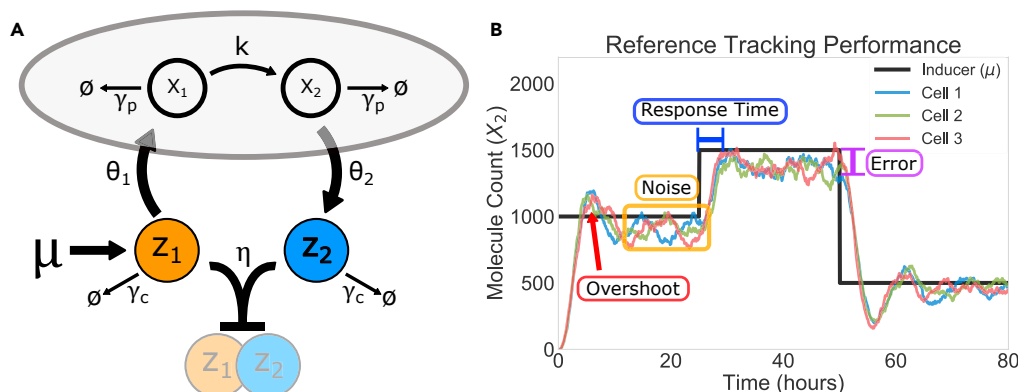https://doi.org/10.1016/j.isci.2019.04.004

**Figure 1. Characterizing Performance in the Antithetic Integral Feedback Circuit**

(A) The circuit diagram for a class of antithetic integral feedback circuits, adapted from the model presented in Briat et al. (2016). Here we take $X_1$ and $X_2$ as the process species we are trying to control and $Z_1$ and $Z_2$ as the controller species. One notable addition is that we explicitly model degradation of the control species $Z_1$ and $Z_2$ at the rate $\gamma_c$. $\theta_1$ and $\theta_2$ represent the interconnection between the process species and the control species, $k$ represents the $X_1$-dependent synthesis rate of $X_2$, and $\gamma_p$ is the degradation rate of the process species. Finally, $\mu$ acts as an external reference that determines production of $Z_1$ through which we would like to ultimately control the steady-state concentration of $X_2$ and $\eta$ is the rate at which $Z_1$ and $Z_2$ irreversibly bind to each other.

(B) A representative plot of the type of behavior we expect from the circuit, where the concentration of $X_2$ tracks a changing reference $\mu$. We see that different cells have the same overall behavior, but with slight variations due to noise. This plot highlights the performance characteristics of this particular implementation of the circuit. For example we see that, when tracking the reference, $X_2$ has some overshoot of the target (red), a period of time it takes to respond to changes (blue), random fluctuations due to noise (yellow), and steady-state error (purple). Ideally, we would like to have a rational methodology to tune the circuit-level parameters of (A) to predictably control the system-level characteristics of (B).

The key property of this circuit is that it is able to implement robust perfect adaptation. This means that, at steady state, the concentration of $X_2$ will be proportional to the reference $\mu$ (specifically, $x_2 = \mu/\theta_2$ on average). Importantly, the steady-state value of $X_2$ will be *independent* of every other parameter of the network, implying that its steady-state behavior is robust. We will focus first on studying a deterministic ordinary differential equation model of the circuit:

$$\dot{x}_1 = \theta_1 z_1 - \gamma_p x_1, \qquad \text{(Equation 1a)}$$
$$\dot{x}_2 = k x_1 - \gamma_p x_2, \qquad \text{(Equation 1b)}$$
$$\dot{z}_1 = \mu - \eta z_1 z_2 - \gamma_c z_1, \qquad \text{(Equation 1c)}$$
$$\dot{z}_2 = \theta_2 x_2 - \eta z_1 z_2 - \gamma_c z_2. \qquad \text{(Equation 1d)}$$

Here $\theta_1$, $\theta_2$, and $k$ are production rates; $\gamma_p$ and $\gamma_c$ are degradation rates for the process species and controller species, respectively; $\eta$ is the rate at which $Z_1$ and $Z_2$ sequester each other; and $\mu$ is the reference input that sets the synthesis rate of $Z_1$. For simplicity we assume that $X_1$ and $X_2$ share the same degradation rate $\gamma_p$, and likewise for $Z_1$ and $Z_2$ with respect to $\gamma_c$. Depending on the process being modeled, it may be more realistic to the have heterogeneous and potentially nonlinear rates for each species; however, the mathematical results are much simpler and easier to interpret in the setting presented here. We analyze a particular circuit with heterogeneous process degradation in Olsman et al. (2018), and a more general discussion of this problem is presented in Baetica et al. (2018).

We will refer to $X_1$ and $X_2$ as process species, and will focus in particular on $X_2$ as the controlled output of the circuit. We can think of $Z_2$ as making measurements of $X_2$, which are then propagated to $Z_1$, which can indirectly affect the production rate of $X_2$ through $X_1$. The use of lower-case letters for the species in Equation 1 indicates that we are referring to a deterministic quantity (later in the section Noise and Fragility Are Two Sides of the Same Coin we will use upper-case variables to denote random variables).

The structure and content of this article is somewhat unconventional, in that we present both a non-technical treatment of some of the core results in the companion piece, Olsman et al. (2018), and also standalone research results that are not discussed in detail elsewhere. The content of Olsman et al. (2018)
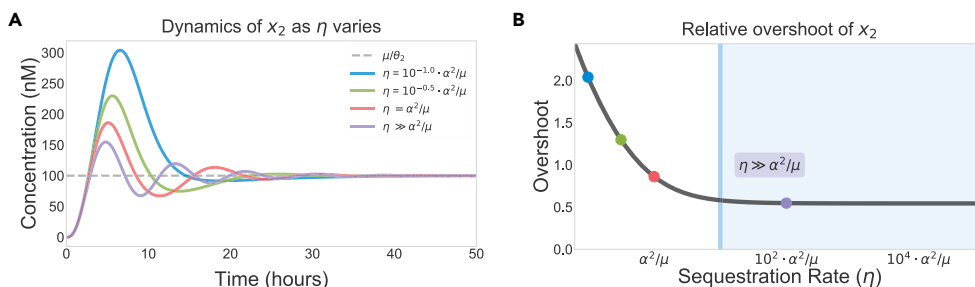
**A** Dynamics of $x_2$ as $\eta$ varies

**B** Relative overshoot of $x_2$

**Figure 2. The Effects of Binding Rate on Dynamics**

(A) Here we show simulations of the circuit in Equation 1 with $k = \theta_1 = \theta_2 = \gamma_P = 1$ h$^{-1}$, $\gamma_c = 0$ h$^{-1}$, and $\mu = 100$ nM h$^{-1}$. This leads to a value of $\alpha^2/\mu = 10^{-2}$ nM$^{-1}$ h$^{-1}$. We vary $\eta$ between $10^{-3}$ and $1$ nM$^{-1}$ h$^{-1}$ and see that for small $\eta$ the system's response is highly sensitive to the binding rate. Once $\eta$ is in the regime described by Equation 3, its dynamics are independent of $\eta$.

(B) A parametric plot showing this phenomenon, using the overshoot of the desired steady-state $x_2^* = \mu/\theta_2$ as a proxy for system performance. The black curve is generated by varying $\eta$ between $10^{-3}$ and $10^3$ nM$^{-1}$ h$^{-1}$, demonstrating that the overshoot becomes almost entirely invariant to $\eta$ in the blue region where $\eta > 10 \cdot \alpha^2/\mu$. The colored dots correspond to the parameters of the simulations in (A).

focuses on the application of classical tools in control theory to study the mathematical properties of the antithetic integral feedback circuit, whereas the goal of this article is to outline practical guidelines that are accessible to an audience interested in utilizing these theoretical results to inform future experimental work in biological engineering.

In Briat et al. (2016), the authors assume that the controller degradation rate $\gamma_c = 0$ in Equations 1c and 1d, which yield the robust precise adaptation mentioned earlier. Our analysis of circuit performance and tradeoffs in the sections Circuit Performance Is Robust to Fast Binding and There Is a Performance Tradeoff between Speed and Robustness makes the same assumption, and we also address the case of $\gamma_c > 0$ in the section Controller Degradation Improves Stability but Introduces Steady-State Error. In the section Antithetic Integral Feedback in a Synthetic Bacterial Growth Control Circuit we apply this analysis to study a particular synthetic growth control circuit that makes use of antithetic integral feedback. Finally, in the section Noise and Fragility Are Two Sides of the Same Coin we will investigate the effects of noise on the circuit.

## RESULTS

### Circuit Performance Is Robust to Fast Binding

The most obvious parameter to investigate in the antithetic integral feedback system is the binding rate $\eta$. To simplify our analysis, we will ignore controller species degradation for the time being ($\gamma_c = 0$ in Equation 1c) and analyze the effect of $\gamma_c$ in later sections. Because binding is a bimolecular interaction, $\eta$ is the rate of association and has units of the form nM$^{-1}$ h$^{-1}$. As the binding of $Z_1$ and $Z_2$ at rate $\eta$ in Equations 1c and 1d encapsulates feedback in the system, we know that $\eta$ cannot be *too* small. If binding is sufficiently slow, it will be as if there is no feedback in the circuit at all. More generally, a small $\eta$ corresponds to a slow feedback action that tends to lead to a large overshoot of the desired steady state, as can be seen in Figure 2A.

The question then becomes, how large should $\eta$ be? Briat et al. (2016) in their original work on this system observed that some sets of parameters lead to unstable behavior (which we discuss in greater depth in Section Instability Arises from Production Outpacing Degradation), so it is important to investigate whether or not a large $\eta$ could ever destabilize the circuit. Ideally, we would like to find a regime of parameters where the system's behavior is easy to predict and we do not have to worry about fine-tuning $\eta$. It would be possible to get a sense for the behavior of $\eta$ by simulating a broad parameter sweep and analyzing the resulting dynamics, whereas we find that it is possible to gain a precise understanding of the effects of $\eta$ via theoretical analysis (described in detail in Olsman et al., 2018).

Before we can analyze the effects of the binding rate on the circuit, we first need some notion of to what quantity it even makes sense to compare $\eta$. If nothing else, this quantity must have the same units as $\eta$,

which immediately rules out a direct comparison with any other rate parameter in Equation 1, as $\eta$ is the only association rate in the system. As $\mu$ is the only other parameter that has units of concentration (specifically nM h$^{-1}$), it must be involved in the comparison. Dimensional analysis can get us as far as noting that a quantity of the form $\alpha^2/\mu$, with $\alpha$ taking units of h$^{-1}$, would at least have same units as $\eta$. This is as far as dimensional analysis alone can take us, because the other parameters in the system ($\theta_1$, $\theta_2$, $k$, and $\gamma_p$) are all rates that have units consistent with $\alpha$.

In Olsman et al. (2018), we find that $\alpha$ should take the form

$$\alpha = \frac{\theta_1 \theta_2 k}{\gamma_p^2}. \qquad \text{(Equation 2)}$$

Although the proof of this result is somewhat technical, we can derive from it a simple guideline for what it means to have $\eta$ large enough. The aggregate quantity $\alpha$ describes the steady-state rate at which $Z_2$ molecules are produced relative to the concentration of $Z_1$. Characterizing the circuit in terms of $\alpha$ may yield practical benefits, as it allows us to sidestep the problem of individually measuring each of the four rate parameters in Equation 2. We will see in later sections that many important features of the circuit can be written either in terms of the individual parameters in Equation 1, or in terms of $\alpha$.

Combining these ideas, we can now state precisely both what it means for $\eta$ to be large and what effect this has on the circuit. We find that, although the behavior of the circuit is highly dependent on the value of all other parameters in the network, it is insensitive to variations in $\eta$, so long as $\eta \gg \max(\alpha, \gamma_p)\alpha/\mu$. As we will discuss later, most of the interesting questions about stability and performance for the system arise when $\alpha$ is at least comparable in scale to $\gamma_p$, so the relevant relationship between $\eta$ and the rest of the parameters in the system can be simplified somewhat to

$$\eta \gg \frac{\alpha^2}{\mu}. \qquad \text{(Equation 3)}$$

This Equation characterizes a separation of timescales between the production and degradation dynamics of the system (captured by $\alpha$ and $\mu$) and the antithetic feedback reaction. Intuitively, so long as binding is sufficiently fast, it does not affect the stability and performance of the circuit's output, $X_2$. This is demonstrated in Figures 2A and 2B, where the system's response becomes independent of $\eta$ when Equation 3 holds. Here we use the amount of relative overshoot of $x_2$ (defined as $x_2^{max}/x_2^* - 1$) as a proxy for characterizing the circuit's behavior.

By simulating the circuit with $\alpha^2/\mu = 10^{-2}$ nM$^{-1}$ hr$^{-1}$ as $\eta$ varies logarithmically between $10^{-3}-10^3$ nM$^{-1}$ hr$^{-1}$, we see in Figure 2B that the behavior of the $x_2$ is insensitive to $\eta$ when it is sufficiently large. The vertical line corresponds to $\eta = 10 \cdot \alpha^2/\mu$. One consequence of Equation 3 is that the steady-state values of $z_1$ and $z_2$ (denoted by *) must have the relationship $z_1^* \gg z_2^*$. If measuring and comparing the rates in Equation 3 is not feasible, it is possible to tell if a circuit described by Equation 1 is in the regime of strong binding by simply comparing the concentrations of $Z_1$ and $Z_2$ at steady state.

We should emphasize that the circuit can still be functional when Equation 3 does not hold; however, our analytic techniques yield less insight into what should be expected from the circuit in this regime. It is also important to note that Equation 3 is not sufficient to guarantee *good* performance (a concept into which we will delve more deeply in later sections). It merely implies that, once $\eta$ is sufficiently large, the qualitative behavior of the $X_2$ (good or bad) will not be affected by varying it. We also note that the dynamics of other species in the network, in particular $Z_1$ and $Z_2$, will be affected by varying $\eta$ even in the strong binding regime. In the next sections, our analysis will focus on the parameter regime where Equation 3 holds and study how the rest of the rates in Equation 1 affect the system's dynamics.

### Instability Arises from Production Outpacing Degradation

A central question for all feedback systems is whether or not the closed-loop circuit is stable. In many engineering applications, it can be the case that poorly implemented feedback control can destabilize an otherwise stable process (Aström and Murray, 2008). This effect is quite salient in the antithetic integral feedback circuit, which was shown to have unstable oscillatory dynamics (known as limit cycles) for some parameter values (Briat et al., 2016). Before we can begin to consider how well a given set of parameters
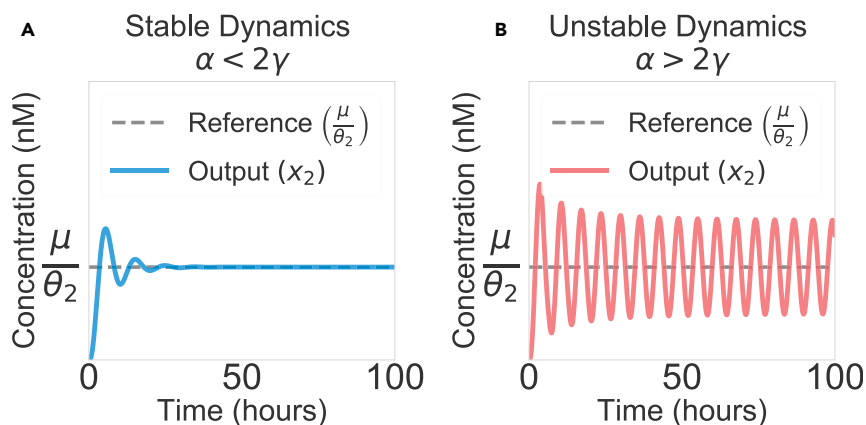
**Figure 3. Dynamics Can Be Either Stable or Unstable**

Here we demonstrate how Equation 4 affects the dynamics of the circuit in Equation 1.

(A) This simulation uses $k = \theta_1 = \theta_2 = \gamma_p = 1$ h$^{-1}$, $\gamma_c = 0$ h$^{-1}$, $\mu = 100$ nM h$^{-1}$, and $\eta = 10$ nM$^{-1}$ h$^{-1}$. We see that $x_2$ shows some transient oscillatory behavior but ultimately adapts the steady-state value $\mu/\theta_2$. As $\alpha = 1$ h$^{-1}$ and $\gamma_p = 1$ h$^{-1}$, Equation 4 holds and the system is stable.

(B) Now we run the simulation with the same parameters, except $\theta_1 = 3$ h$^{-1}$. This implies that $\alpha = 3$ h$^{-1}$, which tells us that Equation 4 no longer holds and the system will become unstable. In this case, the instability takes the form of indefinite oscillations. This figure is adapted from one presented in Olsman et al. (2018).

perform, we first need a guarantee that the corresponding dynamics have the baseline functionality of being stable. Ideally, we would be able to find system-level constraints that determine *a priori* when the circuit will be stable or unstable. Although there exist straightforward numerical methods to predict whether or not a system with a given set of parameters is stable, it is substantially more difficult to derive general parametric conditions that characterize stability.

Take, for example, the relatively simple circuit described in Equation 1, which has seven free parameters. Although it is straightforward to numerically simulate the circuit and investigate different parameter regimes, it is not at all obvious at first glance how the circuit will perform for a particular set of parameter values. We find that in the limit of strong binding and no degradation of $z_1$ and $z_2$, there exists a simple relationship that determines stability. Using the same notation as in the section Circuit Performance Is Robust to Fast Binding, we find that the system is stable if and only if $\alpha < 2\gamma_p$ (as shown in Figure 3). This says that we need the net production rate in the circuit $\alpha$ to be slower than twice the degradation rate $\gamma_p$. We can rewrite this result, using the fact that $\alpha = \theta_1\theta_2 k/\gamma_p^2$, in the form

$$\sqrt[3]{\frac{\theta_1\theta_2 k}{2}} < \gamma_p. \tag{Equation 4}$$

We note that the left-hand term is proportional to the geometric mean of all the production rates in the circuit. This is another perspective from which we can observe that production needs to be, on average, slower than degradation.

An interesting property of this Equation is that $\mu$ and $\eta$ are conspicuously absent. The lack of dependence on $\eta$ echoes the results we discussed in section Circuit Performance Is Robust to Fast Binding, where we showed that the system's performance is independent of the binding rate in the limit of large $\eta$. The fact that the system's stability does not depend on $\mu$ makes sense because it is the only production rate in the system with units of concentration, so it must set the concentration scale for the circuit. We should expect that simply changing the units of concentration in the model should not affect stability. It then follows that varying $\mu$ is analogous to changing the units of concentration, and consequently should not affect stability and performance. We also find that the system is *intrinsically* stable (stable for any set of positive parameters) when there is only one process species in Figure 1A, which we prove in Olsman et al. (2018). We find that for the case of $n > 2$ process species (i.e., the system being controlled consists of species $X_1, \ldots, X_n$) we can derive results analogous to Equation 4, implying that there is a qualitative difference performance between $n = 1$ species and $n \geq 2$ species.

To further investigate Equation 4, we will assume that both the process parameters ($\gamma_P$ and $k$) and the desired set point (determined by $\mu/\theta_2$) are fixed. As we assumed that we are in the regime where $\eta$ is large enough to not matter, the only remaining parameter to tune is $\theta_1$. We can interpret $\theta_1$ as quantifying the strength of interaction between the control species $z_1$ and the process species $x_1$. In this sense, Equation 4 tells us that there is a limit on how strong the connection between the controller and the process can be. It is then natural to ask how varying $\theta_1$ affects the circuits performance. To do this, we first need to define the relevant system-level performance metrics.

### There Is a Performance Tradeoff between Speed and Robustness

In the previous section we noted that, for a given set of parameters, there is a maximum value that $\theta_1$ can take such that the controller remains stable. Picking the rate $\theta_1$ to be fast will speed up the response of the circuit; however, if there is variability in $\theta_1$ the circuit may inadvertently exceed the limit set by Equation 4 and consequently become unstable. In this context, one way to characterize a circuit's robustness is to determine not only if it is stable but also if there are no small parameter changes that would result in it becoming unstable. A robust circuit is one that is far from instability, whereas a fragile circuit will be very near the stability boundary in Equation 4.

It is important to note that the notions of robustness and sensitivity discussed here equivalently capture both the reference tracking behavior (i.e., the ability of $X_2$ to adapt to $\mu/\theta_2$) and rejecting disturbances to modeling parameters (Aström and Murray, 2008). Although we phrase most of the results here and in Olsman et al. (2018) in terms of reference tracking, all the statements about reference tracking have equivalent interpretations in terms of disturbance rejection. We only chose to focus on reference tracking as it is an easier behavior to visualize and intuitively understand. Intuitively if the output of a system is capable of tracking a reference, then we can alternatively think of it as being good at minimizing the error between its current state and its desired state. We can also think of this sort of error minimization as the ability to reject disturbances to parameters. In other words, the ability of the output to robustly track some parameters (in this case, $\mu$ and $\theta_2$) is closely tied to its ability to *not* track other parameters (i.e., reject disturbances).

These observations yield a tradeoff: in order for the response time of the circuit to be as short as possible $\theta_1$ should be fast; however, this necessarily makes the circuit more fragile. This notion of robustness is distinct from robustness of steady state, which is more commonly studied in biological contexts (Barkai and Leibler, 1997; Yi et al., 2000). The steady-state robustness is fairly easy to define, as it is simply the error between the actual steady state of a system and a desired steady state, whereas this notion of fragility requires more sophisticated mathematical tools and is generally difficult to solve for analytically. We discuss these theoretical methods in detail in Olsman et al. (2018), where we show that a good approximation of the fragility of the system has the form

$$\mathcal{F} = \frac{2\gamma_P^3 + \theta_1\theta_2 k}{2\gamma_P^3 - \theta_1\theta_2 k} = \frac{1 + \dfrac{\alpha}{2\gamma_P}}{1 - \dfrac{\alpha}{2\gamma_P}}. \qquad \text{(Equation 5)}$$

An equivalent interpretation of $\mathcal{F}$ is as quantifying the system's worst-case amplification of disturbances. As a sanity check we can see that, when we have equality in Equation 4 (i.e., $\theta_1\theta_2 k = 2\gamma_P^3$), the fragility $\mathcal{F} = \infty$ corresponds to the circuit becoming unstable. When $\theta_1\theta_2 k < 2\gamma_P^3$, $\mathcal{F}$ increases monotonically as $\theta_1$ increases. If $\theta_1 = 0$, then $\mathcal{F} = 1$ corresponding to no disturbance amplification (but also no control). We see in Figure 4A that Equation 5 yields a tradeoff curve that concisely captures the relationship between $\mathcal{F}$ and $\theta_1$.

The upshot of this characterization is that we can now precisely quantify the performance tradeoff between speed and robustness. Equation 4 gave us a binary condition for stability, whereas Equation 5 provides a more nuanced measure of the circuit's performance. Figure 4B demonstrates the effects of this tradeoff on the system's dynamics. We see that, as the initial response time of the system decreases ($\theta_1$ increases), the system begins to oscillate and takes a much longer time to settle in to its steady-state value. These oscillations are indicative of the system approaching instability, a topic we explore in more depth in Olsman et al. (2018).

### Controller Degradation Improves Stability but Introduces Steady-State Error

So far we have neglected the effects of degradation on the control species $z_1$ and $z_2$, assuming that they are only removed from the system by the antithetic binding reaction. Under this assumption, the results of the
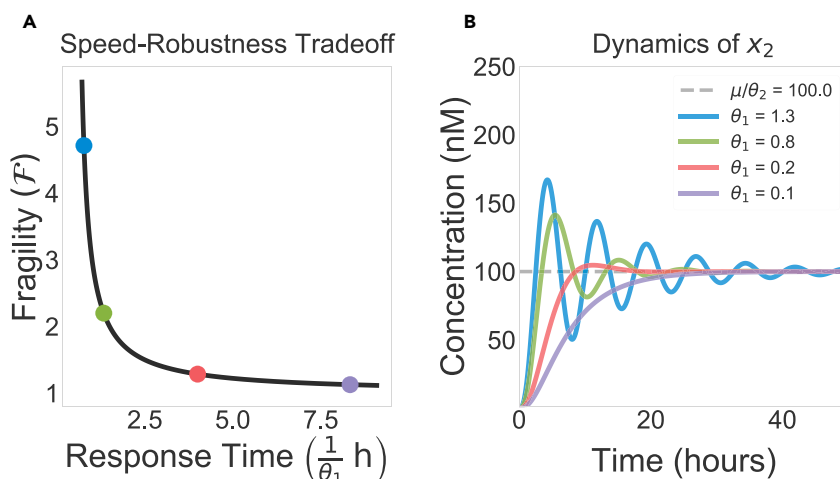
**Figure 4. A Performance Tradeoff between Response Time and Fragility**

(A) Here we show a tradeoff curve demonstrating the relationship between response time (parametrized by $\theta_1^{-1}$) and fragility (as described in Equation 5). An ideal system would have both a fast response and be minimally fragile (i.e., robust), whereas this curve shows that given all other parameters the system only has so much freedom to simultaneously optimize its performance.

(B) These trajectories correspond to parameters associated with the colored dots in (A), showing how fragility and response time relate to the actual dynamics of the circuit. We see that the blue curve rises quickly, but is highly oscillatory and takes a long time to settle. Conversely, the purple curve has a slow rise time, but is quite robust and settles quickly. In each plot we vary $\theta_1$ and use $k = \theta_2 = \gamma_P = 1$ h$^{-1}$, $\gamma_c = 0$ h$^{-1}$, $\mu = 100$ nM h$^{-1}$, and $\eta = 10$ nM$^{-1}$ h$^{-1}$. This figure is adapted from the one presented in Olsman et al. (2018).

previous section tell us that the system is, in a sense, fundamentally constrained in its performance. We might hope, then, that nonzero controller degradation ($\gamma_c > 0$) might give us an additional knob to tune in designing antithetic integral feedback circuits.

This turns out to be precisely the case, as is shown in Figure 5. If all other parameters are held constant, the control species degradation rate $\gamma_c$ decreases the fragility of the system at the cost of introducing steady-state error. Again assuming the limit of large $\eta$, we show in Olsman et al. (2018) that there is a simple expression for this error, which we denote by $\varepsilon$:

$$\varepsilon = \frac{\mu/\theta_2 - x_2^*}{\mu/\theta_2} = \frac{1}{1 + \frac{\alpha}{\gamma_c}}. \tag{Equation 6}$$

We can think of $\varepsilon$ as capturing the steady-state error of $x_2$ relative to the desired set point we would expect in the absence of controller degradation ($\mu/\theta_2$). It is useful to think of controller degradation as adding "leakiness" into the feedback mechanism. Imagine a scenario where $x_2 > \mu/\theta_2$. Ideally, this would cause an increase in $z_2$ that precisely compensates for the mismatch. This increase in $z_2$ will reduce the amount of $z_1$ via antithetic feedback. If, however, $z_1$ is also degraded, there will be two mechanisms through which $z_1$ is removed, namely, degradation and antithetic feedback. If we imagine a scenario in which $\gamma_c$ is extremely large, then every $z_1$ molecule would likely be degraded before having a chance to be sequestered by a $z_2$ molecule. If this were the case, then $x_2$ could not possibly be using feedback to track the set point $\mu/\theta_2$, because there is effectively no way for the increase in $z_2$ to affect the concentration of $z_1$. In Equation 6, we see that $\varepsilon = 0$ if $x_2^* = \mu/\theta_2$ (no error) and $\varepsilon = 1$ when $x_2^* = 0$ (maximum error).

It is also possible to describe the fragility $\mathcal{F}$ for the case where $\gamma_c > 0$. This expression is much more complex than the one presented in Equation 5, so we refer the reader to our analysis in Olsman et al. (2018) for details. The qualitative behavior of $\mathcal{F}$ is shown in Figure 5A, where increasing $\gamma_c$ decreases fragility. Combining these observations, we see that varying controller degradation introduces a tradeoff between steady-state error and robustness. Increasing $\gamma_c$ reduces $\mathcal{F}$ at the cost of increasing $\varepsilon$. Figure 5B demonstrates this effect via simulations of Equation 1 with increasing values of $\gamma_c$. We see that the trajectory with large controller degradation (purple) is far more stable than the trajectory with small degradation (blue); however, the latter differs substantially from the original set point $\mu/\theta_2$.
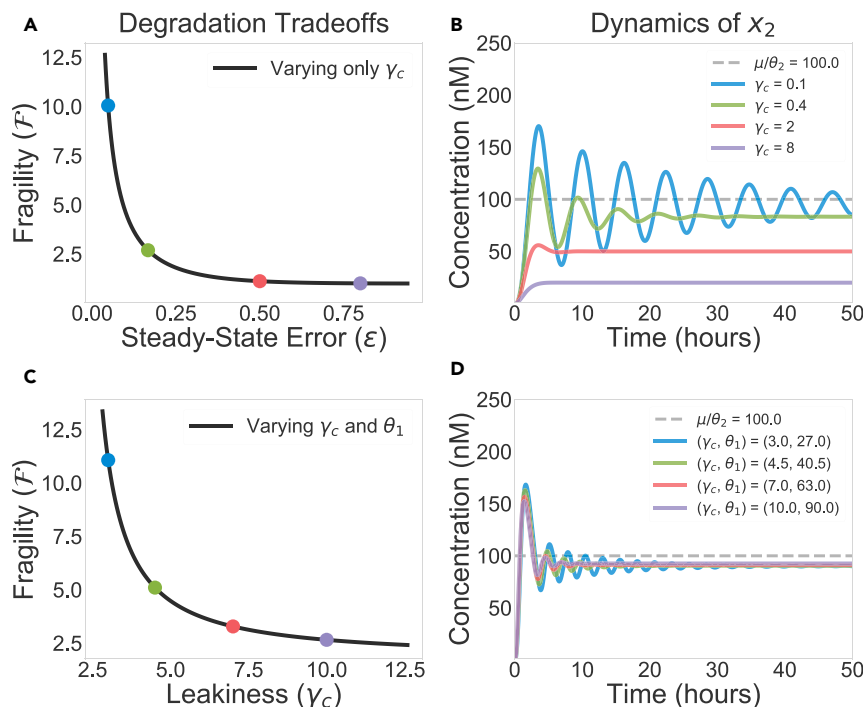
**Figure 5. Controller Degradation Introduces Steady-State Error**

(A) We see that controller degradation $\gamma_c > 0$ improves stability at the cost of introducing steady-state error. This tradeoff curve is a parametric plot where $\gamma_c$ is varied and Equation 6 is compared with a generalization of Equation 5 that incorporates the effects of $\gamma_c$.

(B) Here we show the effects of the tradeoff in (A) on the dynamics of $x_2$. The parameters are chosen such that, if $\gamma_c = 0$, the system would be unstable. The trajectory with small $\gamma_c$ (blue) is stabilized, but still has long-term oscillations indicative of fragility, but has little steady-state error. The trajectory with large $\gamma_c$ (purple) is extremely robust, but with large steady-state error. We vary $\gamma_c$ and use $k = \theta_2 = \gamma_p = 1 \, h^{-1}$, $\theta_1 = 2 \, h^{-1}$, $\mu = 100 \, nM \, h^{-1}$, and $\eta = 300 \, nM^{-1} \, h^{-1}$.

(C) In this tradeoff curve, we hold the error $\varepsilon = 0.1$ constant by varying both $\theta_1$ and $\gamma_c$ as a constant ratio. We now observe that there is a tradeoff between fragility and leakiness, the latter being parameterized by $\gamma_c$. Intuitively, if $\gamma_c$ is large, then many copies of $z_1$ and $z_2$ are being degraded without ever being involved in the feedback process.

(D) We see that simulated trajectories display constant steady-state error, with less oscillatory behavior when $\gamma_c$ is large.

(C and D) use the same parameters as (A and B), with the exception that $\theta_1$ is no longer fixed. This figure is adapted from the one presented in Olsman et al. (2018).

If it were the case that this error were simply a constant offset, then it could, in principle, be corrected for after the fact. The issue, however, is that the error is highly parameter dependent, as can be seen from Equation 6. If the goal is to ensure that the steady-state value of $X_2$ is robust to variation in parameters, this error term may undermine the whole purpose of the circuit. From this perspective, we can think of $\varepsilon$ as capturing the robustness of steady-state behavior of $X_2$ to parametric variations. Ideally, we would have some way to preserve the increased stability from controller degradation without suffering the consequences of large error. Fortunately, this is possible if we vary not only $\gamma_p$ but also the production rate $\theta_1$.

Equation 2 tells us that $\alpha$ is proportional to $\theta_1$. This means that, if we increase $\theta_1$ to match an increase in $\gamma_c$, it would be possible to hold the error in Equation 6 constant. This would not necessarily be very interesting if this increase in $\theta_1$ increased $\mathcal{F}$ by a corresponding amount; however, it turns out that we are still about to decrease $\mathcal{F}$ while keeping the ratio $\theta_1/\gamma_c$ constant, as seen in Figure 5C. We see in Figure 5D this effect in simulations, where each trajectory has a constant steady-state error of $\varepsilon = 0.1$; however, the trajectory with larger $\gamma_c$ values are significantly less oscillatory. This tells us that, if high turnover of $Z_1$ and $Z_2$ is not too costly, it is possible to mitigate the downside of degradation while preserving its benefits.

An interesting property of the dynamics in Figure 5D is that the rise time and overshoot of each trajectory is approximately the same. This is likely a by-product of the fact that the values of $\theta_1$ in these simulations is

large relative to the other production rates in the system. Once $\theta_1$ is sufficiently large, the other $k$ and $\theta_2$ become the rate-limiting reactions, and marginal increases in $\theta_1$ essentially act on a fast timescale that does not have a large effect on the initial transient response of the system. The results of the sections There Is a Performance Tradeoff between Speed and Robustness and Controller Degradation Improves Stability but Introduces Steady-State Error focus on one-dimensional tradeoff curves, with the goal of presenting simple parametric relationships that constraint the possible behavior of the system. This analysis is inherently simplified, as it presents a low-dimensional slice of a high-dimensional space of parameter-system performance relationships. In Baetica et al. (2018) a more general view of these relationships is presented, focusing on surfaces in parameter space and their relationship to system performance.

### Antithetic Integral Feedback in a Synthetic Bacterial Growth Control Circuit

The results presented so far have focused on the simple model of antithetic integral feedback presented in Figure 1. This approach has facilitated our development of theoretical results that characterize some of the important features of antithetic feedback as a mechanism for biological control. We will now make use of the insights gained from the simplified model to study a particular synthetic bacterial growth control circuit. We show that the conceptual guidelines developed so far yield practical insight into the design of this circuit. Specifically, we find that the incorporation of controller degradation can lead to dramatically improved performance. The mathematical details of this analysis are presented in Olsman et al. (2018); here will show simulation results and explain at a high level how the theory can help guide circuit design.

A diagram of the circuit architecture is presented in Figure 6A, where growth control is achieved by regulating the production of the toxin CcdB. Conceptually, if the intracellular concentration of toxin is proportional to the total number of cells, then the population as a whole will converge to a steady-state size that is less than the carrying capacity of the environment. The circuit uses a quorum-sensing mechanism (involving the autoinducer $N$-Acyl homoserine lactone [AHL]) to implement the coupling between population size and CcdB expression. The circuit described so far is capable of constant regulation but lacks an extracellular mechanism through which we can control the population size (assuming that we do not want to be directly tuning protein expression, for example, by altering the strength of ribosome-binding sites).

The desired control can be implemented with antithetic feedback. For simplicity we will focus our modeling efforts on the particular mechanism of sense RNA-antisense RNA (asRNA) pairing; however, it would also be feasible to implement feedback with sigma factor-antisigma factor binding or toxin-antitoxin binding. An asRNA is one that has a complimentary sequence to a messenger RNA (mRNA) strand. This complementarity allows an asRNA to hybridize with an mRNA and block translation. By controlling the expression of asRNA, it is possible to modulate how responsive CcdB expression is to changes in AHL concentration and thus control the total size of the population. This architecture was originally proposed for experimental purposes in McCardell et al. (2017), and a functionally similar circuit was tested in Scott et al. (2017). We model this circuit with the following set of differential equations:

$$\frac{d}{dt}[\text{CcdB}] = k_p[\text{mRNA}] - \gamma_p[\text{CcdB}] \tag{Equation 7a}$$

$$\frac{d}{dt}N = rN\left(1 - \frac{N}{N_m}\right) - \tau[\text{CcdB}]N \tag{Equation 7b}$$

$$\frac{d}{dt}[\text{mRNA}] = k_R G_a N - \eta[\text{mRNA}][\text{asRNA}] - \gamma_R[\text{mRNA}] \tag{Equation 7c}$$

$$\frac{d}{dt}[\text{asRNA}] = \mu - \eta[\text{mRNA}][\text{asRNA}] - \gamma_R[\text{asRNA}]. \tag{Equation 7d}$$

Quantities of the form [·] represent intracellular concentrations for each cell, and $N$ represents the total number of cells. $N$ follows logistic dynamics with an additional death rate due to toxicity $\tau$ proportional to the concentration of [CcdB] per cell. [CcdB] is a protein that is toxic to the cell; [mRNA] is the corresponding messenger RNA, the transcription of which we model as being induced by a quorum-sensing ligand that is produced at a rate proportional to $N$; and [asRNA] is an asRNA that has a complementary sequence to the CcdB mRNA, thus acting as a sequestering partner. The term $G_a$ captures the gain between $N$ and mRNA induction mediated by the quorum-sensing molecule AHL. We can think of [asRNA] and [mRNA] as representing $Z_1$ and $Z_2$, and the quantities [CcdB] and $N$ as representing $X_1$ and $X_2$. This highlights the generality of the modeling framework in Figure 1A: because we did not make any assumptions about the
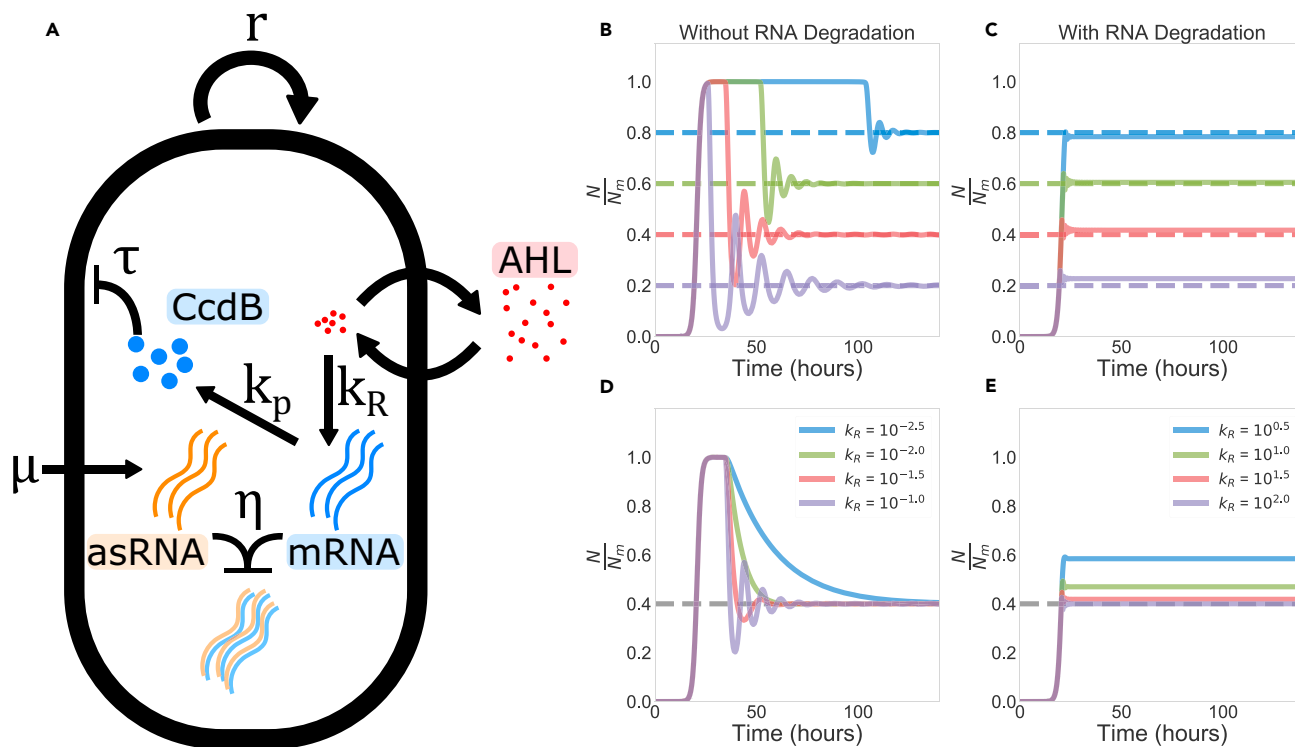
**Figure 6. A Synthetic Growth Control Circuit**

(A) The circuit diagram for the dynamics described in Equation 7.

(B) Simulations of the growth control circuit without RNA degradation (solid lines) for various set points $\mu$ (dashed lines). This architecture exhibits the precise adaptation property, although the response is relatively slow and oscillatory.

(C) Here we see the same circuit simulated with RNA degradation. The response is much faster and more robust; however, there is nonzero steady-state error for each trajectory.

(D) Here we again simulate the circuit without degradation, but now vary $k_R$. We see qualitatively similar performance tradeoffs to those in Figure 4.

(E) As before, we see that adding controller degradation yields a very fast and consistent response. For these particular parameters, the circuit can achieve this performance with relatively little steady-state error. For all circuits we use the parameters $N_m = 10^9$, $r = 1\ \text{h}^{-1}$, $\eta = 20\ \text{nM}^{-1}\ \text{h}^{-1}$, $k_p = 10\ \text{h}^{-1}$, $\gamma_P = 3\ \text{h}^{-1}$, $G_a = 10^{-6}\ \text{nM}$, and $\tau = 4 \times 10^{-3}\ \text{nM}^{-1}\ \text{hr}^{-1}$. (B) uses $k_R = 0.1\ \text{h}^{-1}$ and C uses $k_R = 10\ \text{h}^{-1}$ and $\gamma_R = 20\ \text{h}^{-1}$.

particular nature of the underlying variables, we are able to analyze a circuit with extremely heterogeneous underlying quantities (i.e., RNA, proteins, and cell population).

Figure 6B demonstrates how the growth control circuit adapts to various steady-state population levels when there is no controller degradation ($\gamma_R = 0$). The steady state is set by varying $\mu$. When possible, parameters for this model are taken from You et al. (2004). What is clear across all set points is that the population first grows to carrying capacity before the circuit is activated. Intuitively, the blue curve in Figure 6B has a large amount of asRNA that sequesters mRNA. Because of this, it takes longer to accumulate enough mRNA to make CcdB and lower the population level. In contrast, the purple curve has comparatively little asRNA, effectively increasing the rate at which CcdB can be produced. Qualitatively similar long-term oscillatory behavior in a CcdB-based growth control circuit was observed in Balagaddé et al. (2005).

As You et al. (2004) does not explicitly model transcription, we would ideally pick realistic transcription and translation timescales for bacteria. If we were to naively assume that we could model asRNA and mRNA as if they were directly analogous $Z_1$ and $Z_2$ in the section There Is a Performance Tradeoff between Speed and Robustness, i.e., neglecting controller degradation and assuming they are only removed via strong binding, then we run into an issue. As the antithetic feedback mechanism modeled in the section There Is a Performance Tradeoff between Speed and Robustness assumes that controller degradation is negligible, we must use a very small mRNA synthesis rate to achieve stable dynamics,

assuming all other parameters are fixed in a biologically plausible regime, even if binding is fast. This leads to a slow circuit response and a large transient overshoot. This is demonstrated in Figure 6B, where CcdB production is so slow that the population reaches carrying capacity before the circuit can become active. In Figure 6D we see similar dynamics to those in Figure 4, where the circuit faces harsh tradeoffs between speed and robustness.

We see from Figures 6C and 6E that good performance requires not only that RNA is removed via antithetic feedback but also that it is degraded at a nontrivial rate. At the cost of a lack of precise adaptation, these circuits display dramatically improved performance. In Figures 6C and 6E, the transient overshoot from Figures 6B and 6D has almost entirely disappeared, and each system adapts on a nearly identical timescale, independent of $\mu$. Figures 6D and 6E compare performance for various values of $k_R$ in each system. Figure 6E shows that the introduction of $\gamma_R$ makes the system's dynamics extremely robust to variations in $k_R$ over a wide range of values. We can interpret $\gamma_R$ as introducing a third tradeoff dimension, namely, steady-state error. By allowing the system flexibility along this axis, its speed and robustness are greatly improved.

## Noise and Fragility Are Two Sides of the Same Coin

Our analysis so far has assumed that the underlying circuit is perfectly deterministic, i.e., that its dynamics can be modeled by a system of ordinary differential equations. Although these models serve as a good starting point for studying many biomolecular systems, they do not capture the effects of noise on the system. Although noise is not always an important feature of biological processes, it can sometimes drastically alter the actual behavior of a circuit in a cell (for example, when certain molecules are at a low copy number) (Paulsson, 2005; Lestas et al., 2010).

Here we will examine the steady-state variance of the output species $X_2$ of the antithetic integral feedback system when its dynamics follow a stochastic chemical reaction model and relate it to the performance of the deterministic model Equation 1. The capitalization in $X_2$ reflects that it is now a random variable, whereas $x_2$ in Equation 1b is deterministic. To simplify our analysis, we will return to the assumption that there is no controller degradation ($\gamma_c = 0$). In Briat et al. (2016), the authors observed that there exist parameter values such that the deterministic model is unstable, but the average behavior of the stochastic model is stable (i.e., each species, on average, adapts to the desired steady-state concentration). We might think of each stochastic simulation representing a single cell's dynamics, and the average representing the population-level behavior.

We find that, although this result regarding the mean behavior is correct, it does not tell the whole story. In particular we show that, whereas the population *average* is generally well behaved, the population *variance* can become large. In other words the population as a whole is predictable; however, there is a large amount of cell-to-cell variability at any given time. In fact, it is the case that the noise scales in approximately the same way as the fragility of the system in Equation 5 (as shown in Figure 7A).

Formally, we derive an approximate expression for the steady-state Fano factor (the variance divided by the mean) of $X_2$ in the limit of fast binding:

$$\text{Fano}[X_2] = \frac{\text{Var}[X_2]}{\mathbb{E}[X_2]} \approx \frac{\gamma_P \left(2\theta_1 k + k\gamma_P + 2\gamma_P^2\right)}{2\gamma_P^3 - \theta_1\theta_2 k} \quad \text{(Equation 8)}$$

We see in Figure 7A that the variability of $X_2$ increases as the deterministic system approaches instability. This illustrates that there is a fundamental tradeoff such that the system can be either fast and noisy or slow and accurate, mirroring the deterministic tradeoff described in Figure 4. We can get a sense for why this happens by observing that the denominator in Equation 8 is the same as the denominator of Equation 5. This tells us that we can expect each expression to grow in the same way as the respective denominators approach 0. Thus there is an intimate connection between the sensitivity of the deterministic antithetic integral feedback system, which corresponds to oscillatory behavior, and the sensitivity of the stochastic antithetic integral feedback system, which corresponds to increased noise. To give a more concrete sense for this relationship, we present representative simulation results that demonstrate this behavior.

In Figure 7B, we see that a slow and robust deterministic performance (in the sense described in the section There Is a Performance Tradeoff between Speed and Robustness) corresponds to a stochastic model
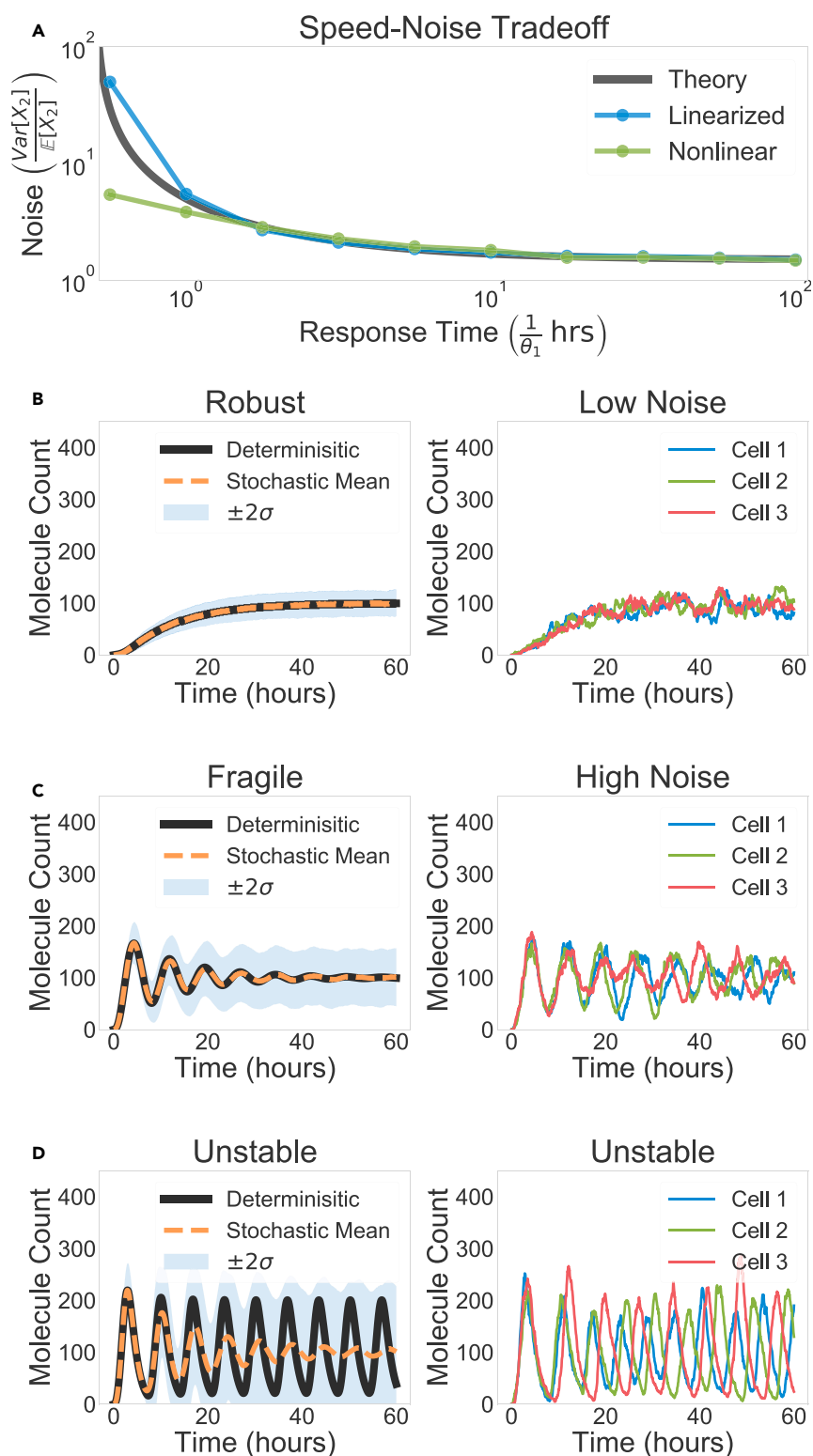
**Figure 7. The Relationship between Noise and Robustness**

(A) Here we see a general tradeoff between response time and noise (quantified by the Fano factor) of the antithetic integral feedback network. This is analogous to the tradeoff in Figure 4A. The plot demonstrates the approximate

**Figure 7. *Continued***

behavior of Equation 8 (black), simulation results for the same approximate model (blue), and simulation results for the fully nonlinear model without approximations (green).

(B) For $\theta_1 = 0.75$ h$^{-1}$, the deterministic and stochastic means converge with good performance; individual stochastic trajectories are not very noisy.

(C) For $\theta_1 = 1.3$ h$^{-1}$, the deterministic and stochastic mean have damped oscillations; individual stochastic trajectories are noisy.

(D) For $\theta_1 = 3.5$ h$^{-1}$, the deterministic model is unstable and oscillates, whereas the stochastic mean is stable, as demonstrated in Briat et al. (2016). We see, however, that the individual trajectories oscillate with randomized phase. In all simulations $k = \theta_2 = \gamma_p = 1$ h$^{-1}$, $\eta = 10$ nM$^{-1}$ h$^{-1}$. In A we use $\mu = 10$ nM h$^{-1}$ to speed up simulations and $\mu = 100$ nM h$^{-1}$ in the remaining panels. Mean trajectories and standard deviations are computed using $N = 1000$ trajectories.

with low noise. The left panel shows the mean behavior matching closely to the deterministic trajectory, with a fairly small amount of noise throughout the simulations. The right panel displays some sample individual trajectories, which essentially look like we would expect: closely following the mean with small deviations. If we look at Figure 7C, we see that the deterministic model and the mean of the stochastic model converge to the reference quickly, with damped oscillations. Just as the fragility of the deterministic system is larger in the left panel, we see that the corresponding noise in the stochastic system is much larger than in Figure 7B. Just as speed increased the fragility in the section There Is a Performance Tradeoff between Speed and Robustness, it appears to increase the variability here. We note that these results assume that the antithetic reactions constitute the only feedback in the system; recent work has shown that additional feedback loops can potentially serve to reduce noise (Briat et al., 2018). In the Supplemental Information we comment on the relationship between our results and those presented in Briat et al. (2018).

Finally, Figure 7D demonstrates a parameter regime where the deterministic model becomes unstable. In the left panel we see precisely the type of behavior described by Briat et al. (2016), where the stochastic mean appears to converge despite deterministic instability. The right panel, however, demonstrates that each individual trajectory is in fact exhibiting noisy oscillations, but with phases that are randomized relative to one another. Each individual cell is unstable, but this instability averages out at the population level. This highlights the importance of distinguishing between average and individual behavior.

## DISCUSSION

Although we could have, in principle, made some of the qualitative observation presented in this work from simulations alone, it is important to emphasize the fact that these theoretical results not only formalize numerical observations but also force us to state exactly what it is we are measuring. An important contribution from Briat et al. (2016) was not only that the authors proposed a clever mechanism to implement feedback control in biological contexts but also went to great effort to clearly state and prove the existence of the fact that the circuit is capable of achieving what they claimed. Our work here and in Olsman et al. (2018) is an attempt to pursue this line of reasoning and further characterize the qualitative and quantitative behavior of this circuit architecture.

More generally, this theoretical perspective sheds light on a variety of nontrivial parameter relationships, which we hope will allow researchers to avoid the need for brute-force parameter tuning when designing future control circuits. This article was intended to provide a relatively non-technical description of the work, and the interested reader can find a great deal more mathematical depth and generality in Olsman et al. (2018). We believe that this an exciting time for biology, where theory and experiment can productively guide each other toward new and interesting directions of inquiry.

## LIMITATIONS OF STUDY

An important technical caveat is that the results presented in this article are derived with respect to linearizations of nonlinear circuits. A more technical discussion of the benefits and limitations of this approach is presented in Olsman et al. (2018); however, the general takeaway is that the linearized theory gives a rigorous treatment of how a circuit behaves near its steady-state values, often referred to as local behavior, much in the same way that the derivative describes the local behavior of a function near a particular point.

Because the goal of a control system is to regulate the dynamics of a process, it is often sufficient to understand the behavior of the system in the local neighborhood near the equilibrium to which we would like the system to adapt. However, it is worth noting that the global behavior on nonlinear systems can sometimes be substantially different from that of its linearization. This appears not to be an impediment for the results presented in this article, as the linearized theory does well to predict the qualitative behavior of nonlinear simulations; however, it is important to make explicit the assumptions that underlie our results. The upshot of pursuing a linearized theory is that there is a broad array of theoretical tools that have been developed to analyze linear systems, and they are both more general and easier to use than most results for nonlinear systems. A more general perspective on the role of linearization in systems biology is presented in Malleshaiah and Gunawardena (2016).

## METHODS

All methods can be found in the accompanying Transparent Methods supplemental file.

## SUPPLEMENTAL INFORMATION

Supplemental Information can be found online at https://doi.org/10.1016/j.isci.2019.04.004.

## AUTHOR CONTRIBUTIONS

N.O. and F.X. conceived of and performed analysis, wrote the manuscript, and wrote code for simulations and figures. J.C.D. supervised the work, gave feedback on the manuscript, and provided funding. Data S1 is provided, which was used to generate the figures in the paper.

## DECLARATION OF INTERESTS

The authors declare no competing interests.

## REFERENCES

Agrawal, D.K., Tang, X., Westbrook, A., Marshall, R., Maxwell, C.S., Lucks, J., Noireaux, V., Beisel, C.L., Dunlop, M.J., and Franco, E. (2018). Mathematical modeling of RNA-based architectures for closed loop control of gene expression. ACS Synth. Biol. *7*, 1219–1228.

Aström, K.J., and Murray, R.M. (2008). Feedback Systems: An Introduction for Scientists and Engineers (Princeton University Press).

Baetica, A.-A., Leong, Y.P., Olsman, N., and Murray, R.M. (2018). Design guidelines for sequestration feedback networks. Biorxiv. https://www.biorxiv.org/content/early/2018/10/30/455493.

Balagaddé, F.K., You, L., Hansen, C.L., Arnold, F.H., and Quake, S.R. (2005). Long-term monitoring of bacteria undergoing programmed population control in a microchemostat. Science *309*, 137–140.

Barkai, N., and Leibler, S. (1997). Robustness in simple biochemical networks. Nature *387*, 913.

Briat, C., Gupta, A., and Khammash, M. (2016). Antithetic integral feedback ensures robust perfect adaptation in noisy biomolecular networks. Cell Syst. *2*, 15–26.

Briat, C., Gupta, A., and Khammash, M. (2018). Antithetic proportional-integral feedback for reduced variance and improved control performance of stochastic reaction networks. J. R. Soc. Interface *15*, 20180079.

Cardinale, S., and Arkin, A.P. (2012). Contextualizing context for synthetic biology—identifying causes of failure of synthetic biological systems. Biotechnol. J. *7*, 856–866.

Chandra, F.A., Buzi, G., and Doyle, J.C. (2011). Glycolytic oscillations and limits on robust efficiency. Science *333*, 187–192.

Cohen-Saidon, C., Cohen, A.A., Sigal, A., Liron, Y., and Alon, U. (2009). Dynamics and variability of ERK2 response to EGF in individual living cells. Mol. Cell *36*, 885–893.

Del Vecchio, D., and Murray, R.M. (2015). Biomolecular Feedback Systems (Princeton University Press Princeton).

Doyle, J.C., Francis, B.A., and Tannenbaum, A.R. (2013). Feedback Control Theory (Courier Corporation).

El-Samad, H., Kurata, H., Doyle, J., Gross, C., and Khammash, M. (2005). Surviving heat shock: control strategies for robustness and performance. Proc. Natl. Acad. Sci. U S A *102*, 2736–2741.

Elowitz, M.B., and Leibler, S. (2000). A synthetic oscillatory network of transcriptional regulators. Nature *403*, 335–338.

Franco, E., Giordano, G., Forsberg, P.-O., and Murray, R.M. (2014). Negative autoregulation matches production and demand in synthetic transcriptional networks. ACS Synth. Biol. *3*, 589–599.

Goentoro, L., and Kirschner, M.W. (2009). Evidence that fold-change, and not absolute level, of $\beta$-catenin dictates wnt signaling. Mol. Cell *36*, 872–884.

Hamilton, A.J., and Baulcombe, D.C. (1999). A species of small antisense rna in posttranscriptional gene silencing in plants. Science *286*, 950–952.

Hsiao, V., de Los Santos, E.L., Whitaker, W.R., Dueber, J.E., and Murray, R.M. (2014). Design and implementation of a biomolecular concentration tracker. ACS Synth. Biol. *4*, 150–161.

Kampranis, S.C., Howells, A.J., and Maxwell, A. (1999). The interaction of DNA gyrase with the bacterial toxin CCDB: evidence for the existence of two gyrase-ccdb complexes. J. Mol. Biol. *293*, 733–744.

Lestas, I., Vinnicombe, G., and Paulsson, J. (2010). Fundamental limits on the suppression of molecular fluctuations. Nature *467*, 174–178.

Lillacci, G., Aoki, S.K., Schweingruber, D., and Khammash, M. (2017). A synthetic integral feedback controller for robust tunable regulation in bacteria. Biorxiv. https://www.biorxiv.org/content/early/2017/08/01/170951.

Lillacci, G., Benenson, Y., and Khammash, M. (2018). Synthetic control systems for high performance gene expression in mammalian cells. Nucleic Acids Res. 46, 9855–9863.

Malleshaiah, M., and Gunawardena, J. (2016). Cybernetics, redux: an outside-in strategy for unraveling cellular function. Dev. Cell *36*, 2–4.

McCardell, R.D., Huang, S., Green, L.N., and Murray, R.M. (2017). Control of bacterial population density with population feedback and molecular sequestration. Biorxiv. https://www.biorxiv.org/content/early/2017/11/25/225045.

Nevozhay, D., Adams, R.M., Murphy, K.F., Josić, K., and Balázsi, G. (2009). Negative autoregulation linearizes the dose–response and suppresses the heterogeneity of gene expression. Proc. Natl. Acad. Sci. U S A *106*, 5123–5128.

Olsman, N., Baetica, A.-A., Xiao, F., Leong, Y.P., Doyle, J., and Murray, R. (2018). Hard limits and performance tradeoffs in a class of sequestration feedback systems. Biorxiv. https://www.biorxiv.org/content/early/2018/09/26/222042.

Paszek, P., Ryan, S., Ashall, L., Sillitoe, K., Harper, C.V., Spiller, D.G., Rand, D.A., and White, M.R. (2010). Population robustness arising from cellular heterogeneity. Proc. Natl. Acad. Sci. U S A *107*, 11644–11649.

Paulsson, J. (2004). Summing up the noise in gene networks. Nature *427*, 415–418.

Paulsson, J. (2005). Models of stochastic gene expression. Phys. Life Rev. *2*, 157–175.

Potvin-Trottier, L., Lord, N.D., Vinnicombe, G., and Paulsson, J. (2016). Synchronous long-term oscillations in a synthetic gene circuit. Nature *538*, 514.

Qian, Y., and Del Vecchio, D. (2018). Realizing integral control in living cells: how to overcome leaky integration due to dilution? J. R. Soc. Interface *15*.

Qian, Y., McBride, C., and del Vecchio, D. (2018). Programming cells to work for us. Annu. Rev. Control Robot Auton. Syst. *1*, 411–440.

Scott, S.R., Din, M.O., Bittihn, P., Xiong, L., Tsimring, L.S., and Hasty, J. (2017). A stabilized microbial ecosystem of self-limiting bacteria using synthetic quorum-regulated lysis. Nat. Microbiol. *2*, 17083.

Sun, Z.Z., Yeung, E., Hayes, C.A., Noireaux, V., and Murray, R.M. (2013). Linear dna for rapid prototyping of synthetic biological circuits in an escherichia coli based tx-tl cell-free system. ACS Synth. Biol. *3*, 387–397.

Swain, P.S., Elowitz, M.B., and Siggia, E.D. (2002). Intrinsic and extrinsic contributions to stochasticity in gene expression. Proc. Natl. Acad. Sci. U S A *99*, 12795–12800.

Weber, E., Engler, C., Gruetzner, R., Werner, S., and Marillonnet, S. (2011). A modular cloning system for standardized assembly of multigene constructs. PLoS One *6*, e16765.

Yi, T.-M., Huang, Y., Simon, M.I., and Doyle, J. (2000). Robust perfect adaptation in bacterial chemotaxis through integral feedback control. Proc. Natl. Acad. Sci. U S A *97*, 4649–4653.

You, L., Cox, R.S., III, Weiss, R., and Arnold, F.H. (2004). Programmed population control by cell-cell communication and regulated killing. Nature *428*, 868.

Zhou, Y., and Gottesman, S. (1998). Regulation of proteolysis of the stationary-phase sigma factor RpoS. J. Bacteriol. *180*, 1154–1158.

**Supplemental Information**

**Architectural Principles for Characterizing**

**the Performance of Antithetic**

**Integral Feedback Networks**

Noah Olsman, Fangzhou Xiao, and John C. Doyle

# Supporting Information

## Analysis of Stochastic Systems

In this section we derive the approximate expression for the Fano factor of the output species in a stochastic antithetic integral feedback system with two process species. In the following we start from the chemical reaction network description of the antithetic integral feedback system (Gillespie (1977, 2000); Munsky and Khammash (2006)), write down the chemical master equation for the stochastic system, and perform approximations with justifications to obtain an expression for the Fano factor of the output species. The approximation used is mathematically the same as the so-called linear noise approximation or first order system size expansion (Paulsson (2005)).

We describe the biochemical reactions of anthithetic integral feedback system with two process species:

$$\emptyset \xrightarrow{\mu} Z_1 \qquad Z_1 \xrightarrow{\theta_1} Z_1 + X_1 \qquad X_1 \xrightarrow{k} X_1 + X_2 \qquad X_2 \xrightarrow{\theta_2} X_2 + Z_2$$

$$X_1 \xrightarrow{\gamma_p} \emptyset \qquad X_2 \xrightarrow{\gamma_p} \emptyset$$

$$Z_1 + Z_2 \xrightarrow{\eta} \emptyset.$$

If we assume infinitely strong binding of the anthithetic integral reaction, then limit $\eta \to \infty$ holds. Hence, at any time, only one of species $Z_1$ and $Z_2$ can be non-zero. If both species are non-zero, then they sequester each other infinitely fast through reaction $Z_1 + Z_2 \to \emptyset$ until one of them becomes zero. Therefore, we can define variable $Z = Z_1 - Z_2$, which has a one-to-one correspondence to species $Z_1$ and $Z_2$ counts, where positive $Z$ indicates counts of $Z_1$, and negative $Z$ indicates counts of $Z_2$.

With this simplification, the dynamics of the stochastic anthithetic integral feedback system can be described by a continuous-time Markov chain (CTMC) over the counts of species $Z$, $X_1$ and $X_2$ using the following master equation dynamics Del Vecchio and Murray (2015):

$$
\begin{aligned}
\dot{p}(x_1, x_2, z) = {} & \mu(p(x_1, x_2, z - 1) - p(x_1, x_2, z)) \\
& + \theta_1 \max\{z, 0\}[p(x_1 - 1, x_2, z) - p(x_1, x_2, z)] \\
& + kx_1[p(x_1, x_2 - 1, z) - p(x_1, x_2, z)] \\
& + \theta_2 x_2[p(x_1, x_2, z + 1) - p(x_1, x_2, z)] \\
& + \gamma_p[(x_1 + 1)p(x_1 + 1, x_2, z) - x_1 p(x_1, x_2, z)] \\
& + \gamma_p[(x_2 + 1)p(x_1, x_2 + 1, z) - x_2 p(x_1, x_2, z)],
\end{aligned}
\tag{1}
$$

where $p(x_1, x_2, z; t)$ denotes the probability for the system to have $Z = z$, $X_1 = x_1$, and $X_2 = x_2$ at time $t$. Here we use the convention that $p(x_1, x_2, z) = 0$ whenever $x_1 < 0$ or $x_2 < 0$. Note that $z$ denote the difference between count of species $Z_1$ and $Z_2$, so it can take negative values.

We observe that all the terms on the right hand side of equation (1) are linear, except for the $\max\{z, 0\}$ term. We can see this more clearly if we consider the first moment equation.

If we consider the steady state master equation, we set the left hand side to 0 and we apply $\sum_{x_1,x_2,z} x_1$ with the sum over all $x_1, x_2 \in \mathbb{N}, z \in \mathbb{Z}$, then we obtain that

$$\theta_1 \mathbb{E}(Z|Z \geq 0)\mathbb{P}(Z \geq 0) = \gamma_p \mathbb{E}X_1$$

Similarly, if we apply $\sum_{x_1,x_2,z} x_2$, and $\sum_{x_1,x_2,z} z$, we get

$$k\mathbb{E}X_1 = \gamma_p \mathbb{E}X_2 \qquad \mu = \theta_2 \mathbb{E}X_2.$$

The term that prevents us from solving this set of linear equations for the first moments is the $\max\{z, 0\}$ term, which results in the probability for $Z$ to be non-negative in the moment equations.

Therefore, we make a second assumption that $Z \geq 0$ with probability 1 at steady state. This means $Z_2$ is zero with probability 1 and this represents a good approximation if the system is stable, without $Z_1$ oscillating to a very low count.

Under this assumption, we then obtain the linear equation:

$$\theta_1 \mathbb{E}Z = \gamma_p \mathbb{E}X_1.$$

Similarly, if we apply sum $\sum_{x_1,x_2,z} x_1 z$ to the master equation, we obtain a system of linear equations for steady-state moments of both the first and the second order terms. As the system of equations becomes cumbersome to solve by hand, a Mathematica script was written to automatically derive and solve the moment equations. Solution gives the Fano factor of $x_2$ as the following:

$$\frac{\text{Var}\,X_2}{\mathbb{E}X_2} = \frac{\gamma_p(2\theta_1 k + k\gamma_p + 2\gamma_p^2)}{2\gamma_p^3 - \theta_1\theta_2 k}. \tag{2}$$

As $\gamma_p \to \infty$, we obtain an additional simplification

$$\frac{\text{Var}\,X_2}{\mathbb{E}X_2} \sim 1 + \frac{k}{2\gamma_p}.$$

It should be noted that while the Fano factor result derived above are the same as the recent results in Briat et al. (2018), the method of derivation and the insights that can be obtained are different. Where Briat et al. (2018) derived results using moment invariants from the chemical master equation of the full system without the large $\eta$ assumption to highlight the invariant properties of the antithetic integral feedback system, we used the large $\eta$ assumption to derive a simplified chemical master equation equation (1) that highlights the almost-linear property of the system. It further suggests that the only nonlinearity, $\max\{z, 0\}$, which acts like a saturation effect, is the central nonlinearity that differentiates the full model of antithetic integral feedback from its linearization. We mean this in the sense that, when the system is far from saturation, the linear and nonlinear models exhibit the same behavior. The linearization appears to break down when $Z$ frequently becomes negative.

On a more philosophical level, we note that both our result here and the result in Briat et al. (2018) can be calculated by brute-force using the linear noise approximation Paulsson (2005), however the specific derivations and arguments here and in Briat et al. (2018) provide insight about the system beyond the resulting equation.

# References

Briat, C., Gupta, A., Khammash, M., 2018. Antithetic proportional-integral feedback for reduced variance and improved control performance of stochastic reaction networks. Journal of The Royal Society Interface 15 (143), 20180079.

Del Vecchio, D., Murray, R. M., 2015. Biomolecular feedback systems. Princeton University Press Princeton, NJ.

Gillespie, D. T., 1977. Exact stochastic simulation of coupled chemical reactions. The journal of physical chemistry 81 (25), 2340–2361.

Gillespie, D. T., 2000. The chemical langevin equation. The Journal of Chemical Physics 113 (1), 297–306.

Munsky, B., Khammash, M., 2006. The finite state projection algorithm for the solution of the chemical master equation. The Journal of chemical physics 124 (4), 044104.

Paulsson, J., 2005. Models of stochastic gene expression. Physics of life reviews 2 (2), 157–175.